New Phases of Water Ice Predicted at Megabar Pressures

Burkhard Militzer[1,2] and Hugh F. Wilson[1]

[1]*Department of Earth and Planetary Science*
[2]*Department of Astronomy, University of California, Berkeley*

Based on density functional calculations we predict water ice to attain two new crystal structures with *Pbca* and *Cmcm* symmetry at 7.6 and 15.5 Mbar, respectively. The known high pressure ice phases VII, VIII, X, and *Pbcm* as well as the *Pbca* phase are all insulating and composed of two interpenetrating hydrogen bonded networks, but the *Cmcm* structure is metallic and consists of corrugated sheets of H and O atoms. The H atoms are squeezed into octahedral positions between next-nearest O atoms while they occupy tetrahedral positions between nearest O atoms in the ice X, *Pbcm*, and *Pbca* phases.

PACS numbers:

Water ice is one of the most prevalent substances in the solar system, with the majority of it existing at high pressures in the interiors of giant planets [1]. Uranus and Neptune are assumed to consist largely of a mixture of water, ammonia and methane ices at pressures up to 8 Mbar [2], while Jupiter and Saturn almost certainly have large dense cores consisting of differentiated rock and ice components at pressures on the order of 10 Mbar in Saturn [2] and $39-64$ Mbar in Jupiter [3]. The behavior of water ice under these extreme conditions is not yet well understood because static diamond anvil cell experiments have not yet reached beyond 2.1 megabars [4–7]. Shock wave experiments [8] have reached higher pressures but they also heat the sample significantly so that it melts for the highest pressures. However, dynamic ramp compression techniques [9, 10] are expected to reach high pressures at comparatively low temperatures, where so far only theoretical methods have predicted the state of water ice.

The known phase diagram of water is extremely rich, with at least fifteen forms of solid ice observed experimentally [11] and one high-pressure phase predicted theoretically [12]. The high-pressure region of the phase diagram is comparatively simple. The molecular ice VIII phase, which forms at low temperatures for pressures above $\sim$15 kbar, consists of a *bcc* array of oxygen atoms with an ordered arrangement of hydrogen atoms arranged along the tetrahedral directions, bonded with a short covalent bond to one oxygen and a longer hydrogen bond to the other. Increasing pressure to 0.7 Mbar results in the symmetrization of these bonds [13], with the distinction between covalent and hydrogen bonds being lost as the hydrogen occupies the midpoint between the two oxygens. This is referred to as phase X, the highest-pressure phase that has been observed experimentally. In 1996 Benoit *et al.* [12] used density functional theory (DFT) to predict a higher-pressure phase of ice with *Pbcm* symmetry and twelve atoms per unit cell to become stable at approximately 3 Mbar. It was recently shown within DFT that this phase forms by a dynamic instability in the ice X lattice [14, 15].

At temperatures in excess of approximately 2000 K, high-pressure ice transitions to a superionic phase [16–18] in which the hydrogen atoms become mobile while the oxygen atoms do not, while at higher temperatures still the oxygen atoms also become mobile and the entire structure melts [19]. In the recent work by French *et al.* [20] it was shown that the *bcc* structure of the oxygen lattice in the superionic phase appears to be maintained up to very high pressures. This work also indicated that at densities below approximately 5 g cm^{-3}, corresponding to pressures around 6 Mbar, the hydrogen atoms are found to be strongly associated with the four tetrahedral sites surrounding each oxygen as in ice X, but at higher pressures the hydrogen atoms show an increasing preference for the six octahedral sites surrounding around each oxygen. It is thus natural to ask whether the occupation of these sites may lead to the formation of a novel crystalline phase of ice that would be more stable than the *Pbcm* phase at high pressure.

To investigate the plausibility of the occupation of the octahedral sites at low temperature we performed a molecular dynamics simulation in which a superionic water sample in a 48-atom cell at a pressure of approximately 29 Mbar was quenched from a temperature of 5000 K to zero temperature over a period of 2 ps. In this simulation, as with all simulations described later, we used the VASP density functional theory code [21], with pseudopotentials of the projector-augmented wave type [22], a cutoff for the expansion of the plane wave basis set for the wavefunctions of at least 1360 eV, and the PBE exchange-correlation functional [23]. The simulation used an NVT ensemble controlled by a Nose-Hoover thermostat in which the cell vectors were not allowed to change. In the resulting structure, the oxygen atoms retained their *bcc* lattice structure, while the hydrogen atoms all ended up close to the octahedral lattice sites, while none was close to a tetrahedral lattice site. This provides motivation for a more thorough investigation of this class of crystalline structures with octahedral hydrogen occupation.

The *bcc* oxygen lattice provides four tetrahedral sites surrounding each oxygen and lying at the midpoint of the nearest-neighbor pairs, and six octahedral sites lying at the midpoint of second-nearest-neighbor pairs. This gives only one way to occupy the tetrahedral sites with two hydrogen atoms per oxygen, but many ways to occupy the octahedral sites with two hydrogen atoms per oxygen. On the assumption that the stablest configuration was likely to have reasonably high symmetry, we systematically studied each possible configuration of hydrogen atoms for the three smallest possible unit cells: the six-atom $1 \times 1 \times 1$ unit cell, the twelve-atom $2 \times 1 \times 1$

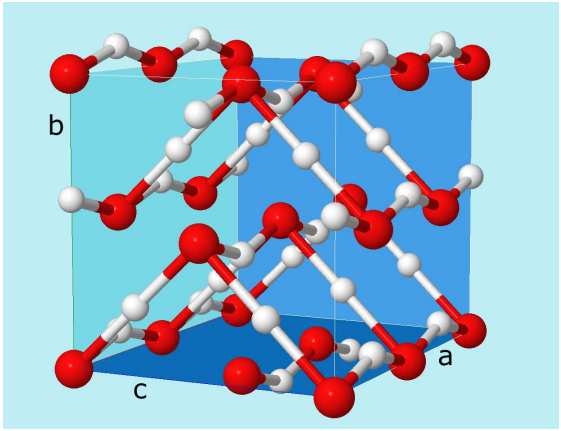

FIG. 1: *Cmcm* ice structures where the large and small spheres denote the oxygen and hydrogen atoms respectively. The orthorhombic unit cell with 12 atoms has been doubled in a direction and shifted so that an oxygen atom is at the origin.

unit cell and the twelve-atom $\sqrt{2} \times \sqrt{2} \times 1$ unit cell. This resulted, after the removal of equivalent structures, in three configurations for the $1 \times 1 \times 1$ unit cell, six configurations for the $2 \times 1 \times 1$ unit cell and also six configurations for the $\sqrt{2}\times\sqrt{2}\times 1$ unit cell. Larger unit cells were found to have impractically large numbers of inequivalent configurations. For each configuration, we performed a full geometry optimization at a pressure of 29 Mbar.

The most stable configuration consists of a $\sqrt{2} \times \sqrt{2} \times 1$ orthorhombic cell with 12 atoms and is shown in Fig. 1. Its reduced coordinates given in Tab. I. The structure has *Cmcm* symmetry and may also be represented in 6-atom monoclinic unit cell with the vectors $a_{\rm m}$=$(a+b)/2$, $b_{\rm m}$=$(a-b)/2$, $c_{\rm m}$=c. This structure is one of a relatively small number of configurations which can be formed by filling two out of every three octahedral lattice sites with hydrogen atoms in such a way that no two vacancies are immediately adjacent. During the structural relaxation, the hydrogen atoms that connect two oxygen atoms along the a direction move up along the b direction ($y = 0.25 \rightarrow 0.34$) towards the third vacant hydrogen site. This elongates their bonds with the nearest oxygen atoms and introduces the kinks into O-H chains that are shown in Fig. 1. The structural relaxation of the next three lowest-enthalpy structures yielded enthalpies which are 0.51, 0.59, and 1.1 eV per H_2O unit higher. We also doubled and quadrupled the unit cell and re-relaxed structure starting with distorted hydrogen positions but no structure with lower enthalpy was found.

The orthorhombic structure with *Cmcm* symmetry is common among high pressure materials including phase II of molecular hydrogen [24], AB and AB_2 compounds, and the post-perovskite phase of ABO_3. A *Cmcm* structure [25] with a four-atom unit cell was also proposed for the ϵ phase of molecular oxygen but experiments later determined a different structure with $C2/m$ symmetry [26].

Prompted by the referee, we also performed lattice dynamics calculations with Abinit [27] and VASP codes. This revealed a dynamic instability in the *Pbcm* structure. Fig. 3 illustrates that the mode $(1/2, 0, 0)$ becomes unstable at 7.6 Mbar. The structural relaxation in a $2 \times 1 \times 1$ unit cell with 24 atoms gave rise to a new intermediate structure of *Pbca* symmetry (Tab. I) that precedes the transition to the *Cmcm* phase in pressure. The resulting sequence is shown in Fig. 2. In the *Pbca* structure, the hydrogen atoms are squeezed out of the

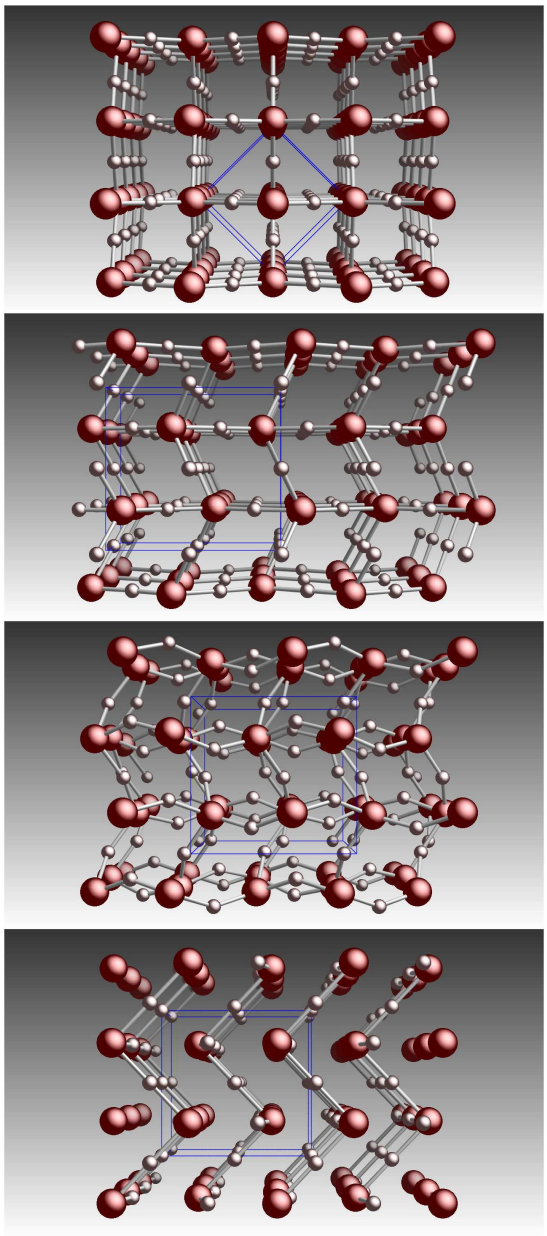

FIG. 2: Structures of the ice X, *Pbcm*, and new *Pbca* and *Cmcm* phases are shown from top to bottom. The large and small spheres denote the O and H atoms respectively, while the thin lines denote the unit cells. The ice X to *Pbcm* transition is a displacement of atomic layers. In *Pbca*, the H atoms are squeezed out of midpoint between nearest O atoms. In *Cmcm*, the H atoms occupy mid-points between next-nearest O atoms.

Symmetry	*Pbca*	*Pnma*	*Cmcm*
Pressure (Mbar)	10.0	12.0	20.0
Density (g cm^{-3})	6.192	6.679	8.115
Atoms in unit cell	24	12	12
a (Å)	3.117	3.005	1.869
b (Å)	3.762	1.925	2.841
c (Å)	3.295	3.098	2.778
H	$c\begin{pmatrix}0.8036\\0.0015\\0.1484\end{pmatrix}$	$c\begin{pmatrix}0.0029\\3/4\\0.2330\end{pmatrix}$	$a\begin{pmatrix}0\\0\\0\end{pmatrix}$
H	$c\begin{pmatrix}0.4862\\0.7161\\0.5370\end{pmatrix}$	$c\begin{pmatrix}0.2870\\3/4\\0.9154\end{pmatrix}$	$c\begin{pmatrix}1/2\\0.8498\\1/4\end{pmatrix}$
O	$c\begin{pmatrix}0.2592\\0.1311\\0.1040\end{pmatrix}$	$c\begin{pmatrix}0.7536\\3/4\\0.0427\end{pmatrix}$	$c\begin{pmatrix}1/2\\0.7237\\3/4\end{pmatrix}$

TABLE I: Structural parameters of different ice phases in orthorhombic unit cells. The last three lines specify the Wyckoff positions and the reduced coordinates of the atoms. The remaining positions follow from symmetry operations.

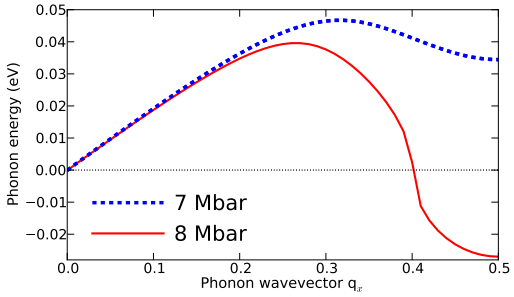

FIG. 3: Dispersion curve of the *Pbcm* phonon band with the lowest energy along the a direction, exhibiting an instability at 7.6 Mbar.

midpoint between two nearest oxygen atoms. However, they still reside near their tetrahedral sites. The distortion of the H positions occurs in alternating directions in the two hydrogen bonded networks, which is accommodated by the unit cell doubling in a direction.

The *Cmcm* structure is distinct from the other high-pressure ice phases in several ways. While ices VII, VIII and X as well as the *Pbcm* and *Pbca* structures all consist of two interpenetrating hydrogen bonded networks, the *Cmcm* structure consists of corrugated sheets of H and O atoms (Figs. 1 & 2). While in lower-pressure structures the hydrogen atoms occupy sites between nearest pairs of oxygen atoms, in the *Cmcm* structure they are squeezed into sites between second-nearest pairs of oxygen atoms. It should be noted that the characterization of crystalline solids in terms of chemical bonds makes less sense at very high pressure because the structures are increasingly dominated by the mutual repulsion of atomic cores rather than the formation of favorable electronic bonds between atoms. The repulsive forces that keep the atoms at their

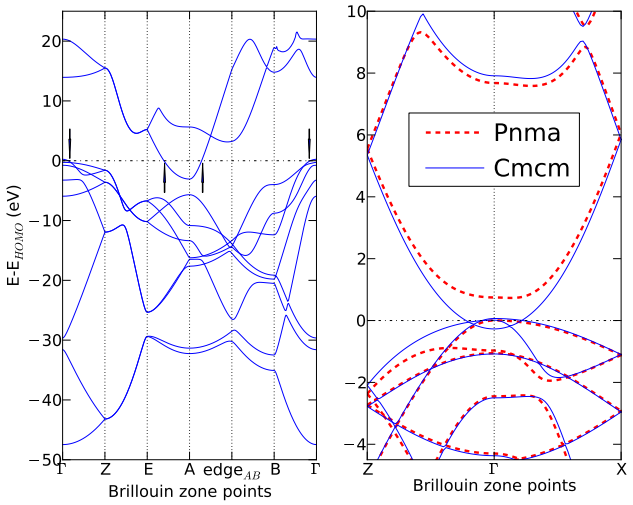

FIG. 4: Left: Electronic band structure for the *Cmcm* phase in a monoclinic unit cell at 22 Mbar. The arrows indicate where bands cross the Fermi level underlining the metallic nature of this phase. Right: Comparison of *Pnma* and *Cmcm* band structures at 12.5 Mbar in the orthorhombic unit cell illustrate the Peierls instability.

lattice sites increase strongly with pressure, however.

Band structure calculations show that the *Cmcm* phase is metallic for all pressures under consideration. Fig. 4 shows that the band which was the conduction band in the lower-pressure structures, now dips below the Fermi level a the A point of the monoclinic cell and becomes partially occupied. Similarly a valence bands becomes unoccupied near Γ.

However, careful structural relaxations in the pressure range of 7.6-15.5 Mbar reveal the existence of a Peierls instability that opens a band gap (Fig. 4) by shifting hydrogen atom slightly away from the mid-point between near-nearest oxygen atoms. This distortion is small and fractional coordinates change by less than 2%. It lowers the enthalpy by just 7 meV per molecule. The resulting structure has *Pnma* symmetry with 12 atoms in an orthorhombic unit cell. Table I lists the structural parameters in the conventional coordinate setting for *Pnma* that differs from that for *Cmcm*.

At 15.5 Mbar the band gap in the *Pnma* structure closes and the mechanism for the Peierls instability disappears. This pressure marks the transition from the *Pnma* to the *Cmcm* structure. Since all lower pressure ice phases are insulating, the transition to *Cmcm* at 15.5 Mbar marks the insulator-to-metal transition in water ice.

We now compare the enthalpy, $H = E + PV$, of the ice X, *Pbcm*, *Pbca*, *Pnma*, and *Cmcm* structure after having optimized the geometry in constant-pressure variable-cell simulations from 5 to 50 Mbar. Figure 5 shows the enthalpy difference of the *static* lattice relative to the *Pbcm* structure. The ice X structure transforms into the *Pbcm* structure for pressures above approximately 3 Mbar, consistent with the results of Benoit *et al.* [12]. The *Pbcm* structure transforms into the *Pbca* phase at 7.6 Mbar consistent with our lattice dynamics calculations.

According to static lattice calculations, the *Pbca* phase would transform into *Cmcm* structure at 17.7 Mbar. To test the importance of zero point motion, we perform lattice dynamics calculation in the harmonic approximation with a $4 \times 4 \times 4$ q point grid. The *Cmcm* and *Pnma* phases have significantly lower zero point energy than the *Pbca* phase (e.g. 75 meV per molecule at 12 Mbar) because the hydrogen atoms are less constrained at their octahedral sites between the more distant next-nearest oxygen atoms, leading to softer phonon modes. The resulting reduction in zero point energy means that the *Pbca* structure transforms into the insulting *Pnma* structure at 12.5 Mbar before this structure changes to *Cmcm* at 15.5 Mbar.

Prompted by the referee, we also tested the validity of the PAW VASP pseudopotentials by performing full-potential all-electron calculation with the *Exciting* code [28]. We focused this test on the *Pbcm*-to-*Cmcm* transition that occurs at 13.1 Mbar (Fig. 5) within the PBE approximation. We recalculated this transition pressure within the local density approximation (LDA) and obtained 11.5 Mbar. Such a pressure difference is not unexpected because LDA typically underestimates transition pressures [29]. We then determined the energy from all-electron calculation for the five geometries in each phase that we obtained with LDA PAW calculations from 9 to 14.3 Mbar. We fit the resulting equations for state for both phases and recalculated the transition pressure. The all-electron method shifted the resulting transition pressure by less than 0.1 Mbar, which confirms that the PAW pseudopotentials are sufficiently accurate for the purpose for this study.

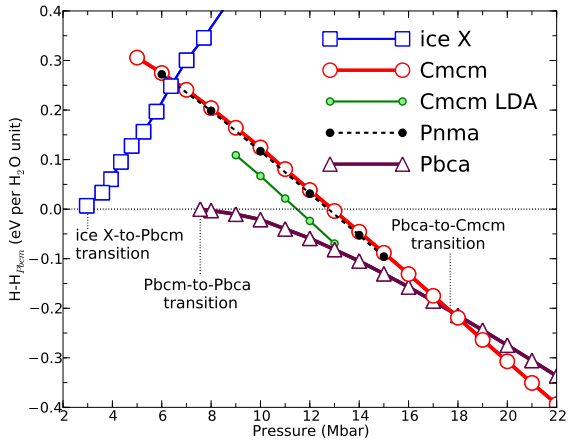

FIG. 5: Enthalpy differences of the ice X, *Pbca*, *Pnma*, and *Cmcm* structures from the *Pbcm* structure as a function of pressure. PBE [23] was used except where LDA is indicated. Results are for static lattices without zero point motion.

We have predicted that water ice will attain novel crystal structures at megabar pressures and determined the following sequence of structural transformations. At 7.6 Mbar the *Pbcm* phase will transform into a *Pbca* phase, which then changes into an insulating *Pnma* structure at 12.5 Mbar. At 15.5 Mbar a insulator-to-metal transition leads to a structure with *Cmcm* symmetry. This last transition is expected to greatly increase reflectivity in water ice, which will make it easier detect with spectroscopic techniques in dynamic high pressure experiments. Ramp compression [9, 10] and pre-compressed [8] shock waves appear as most promising techniques.

[1] W. B. Hubbard. *Planetary Interiors*. University of Arizona Press, Tucson, AZ, 1984.
[2] T. Guillot. *Science*, 286:72, 1999.
[3] B. Militzer, W. H. Hubbard, J. Vorberger, I. Tamblyn, and S. A. Bonev. *Astrophys. J. Lett.*, 688:L45, 2008.
[4] R. J. Hemley *et al. Nature*, 330:737, 1987.
[5] A. F. Goncharov *et al. Science*, 273:218, 1996.
[6] P. Loubeyre, R. LeToullec, E. Wolanin, M. Han, and D. Hausermann. *Nature*, 397:503, 1999.
[7] A. F. Goncharov *et al. J. Chem. Phys.*, 139:124514, 2009.
[8] K. K. M. Lee *et al. J. Chem. Phys.* 125:014701, 2006 and references therein.
[9] J.-P. Davis et al. *Phys. Plasmas*, 12:056310, 2005.
[10] D. H. Dolan, M. D. Knudson, C. A. Hall, and C. Deeney. *Nature*, 3:339, 2007.
[11] C. G. Salzmann, P. G. Radaelli, E. Mayer, and J. L. Finney. *Phys. Rev. Lett.*, 103:105701, 2009.
[12] M. Benoit, M. Bernasconi, P. Focher, and M. Parrinello. *Phys. Rev. Lett.*, 76:2934, 1996.
[13] A. Polian and M. Grimsditch. *Phys. Rev. Lett.*, 52:1312, 1984.
[14] R. Caracas. *Phys. Rev. Lett.*, 101:085502, 2008.
[15] M. Marques, G. J. Ackland, and J. S. Loveday. *High Pressure Res.*, 29:208, 2009.
[16] C. Cavazzoni, G. L. Chiarotti, S. Scandolo, E. Tosatti, M. Bernasconi, and M. Parrinello. *Nature*, 283:44, 1999.
[17] A. F. Goncharov *et al. Phys. Rev. Lett.*, 94:125508, 2005.
[18] T. R. Mattsson and M. P. Desjarlais. *Phys. Rev. Lett.*, 97:017801, 2006.
[19] E. Schwegler, M. Sharma, F. Gygi, and G. Galli. *Proc. Nat. Acad. Sci.*, 105:14779, 2008.
[20] M. French, T. R. Mattsson, N. Nettelmann, and R. Redmer. *Phys. Rev. B*, 79:054107, 2009.
[21] G. Kresse and J. Furthmüller. *Phys. Rev. B*, 54:11169, 1996.
[22] P. E. Blöchl. *Phys. Rev. B*, 50:17953, 1994.
[23] J. P. Perdew, K. Burke, and M. Ernzerhof. *Phys. Rev. Lett.*, 77:3865, 1996.
[24] P. Toledano, H. Katzke, A. F. Goncharov, and R. J. Hemley. *Phys. Rev. Lett.*, 103:105301, 2009.
[25] J. B. Neaton and N. W. Ashcroft. *Phys. Rev. Lett.*, 88:205503, 2002.
[26] L.F. Lundegaard, G. Weck, M. I. McMahon, S. Desgreniers, and P. Loubeyre. *Nature*, 443:443, 2006.
[27] X. Gonze *el at. Comp. Phys. Comm.*, 180:2582, 2009.
[28] J.K. Dewhurst *et al.*, The EXCITING FP-LAPW code, http://exciting.sourceforge.net.
[29] D. R. Hamann. *Phys. Rev. Lett.*, 76:660, 1996.

This work was supported by NASA and NSF. Computational resources were provided in part by NCCS, NERSC, and TAC. We acknowledge discussions with T. Ogitsu, R. Jeanloz, and R. Martin and advice on phonon calculations from S. Stackhouse and I. Souza.